American Journal of Botany

RESEARCH ARTICL

Anatomical and hydraulic responses to desiccation in emergent conifer seedlings

Megan L. Miller[1], Adam B. Roddy[2,3], Craig R. Brodersen[3], Andrew J. McElrone[4,5], and Daniel M. Johnson[6,7]

Manuscript received 30 December 2019; revision accepted 23 April 2020.

[1] Department of Forest, Rangeland, and Fire Sciences, University of Idaho, 875 Perimeter Drive MS 1133, Moscow, ID 83844, USA

[2] Department of Integrative Biology, University of California Berkeley, Berkeley, CA 94720, USA

[3] School of Forestry & Environmental Studies, Yale University, New Haven, CT 06511, USA

[4] Department of Viticulture and Enology, University of California, Davis, CA 95616, USA

[5] USDA-ARS, Davis, CA 95616, USA

[6] Warnell School of Forestry and Natural Resources, University of Georgia, Athens, GA 30602, USA

[7] Author for correspondence (e-mail: danjohnson@uga.edu)

Citation: Miller, M. L., A. B. Roddy, C. R. Brodersen, A. J. McElrone, and D. M. Johnson. 2020. Anatomical and hydraulic responses to desiccation in emergent conifer seedlings. *American Journal of Botany* 107(8): 1–12.

doi:10.1002/ajb2.1517

PREMISE: The young seedling life stage is critical for reforestation after disturbance and for species migration under climate change, yet little is known regarding their basic hydraulic function or vulnerability to drought. Here, we sought to characterize responses to desiccation including hydraulic vulnerability, xylem anatomical traits, and impacts on other stem tissues that contribute to hydraulic functioning.

METHODS: *Larix occidentalis*, *Pseudotsuga menziesii*, and *Pinus ponderosa* (all ≤6 weeks old) were imaged using x-ray computed microtomography during desiccation to assess seedling biomechanical responses with concurrently measured hydraulic conductivity (k_s) and water potential (Ψ) to assess vulnerability to xylem embolism formation and other tissue damage.

RESULTS: In non-stressed samples for all species, pith and cortical cells appeared circular and well hydrated, but they started to empty and deform with decreasing Ψ which resulted in cell tearing and eventual collapse. Despite the severity of this structural damage, the vascular cambium remained well hydrated even under the most severe drought. There were significant differences among species in vulnerability to xylem embolism formation, with 78% xylem embolism in *L. occidentalis* by Ψ of −2.1 MPa, but only 47.7% and 62.1% in *P. ponderosa* and *P. menziesii* at −4.27 and −6.73 MPa, respectively.

CONCLUSIONS: *Larix occidentalis* seedlings appeared to be more susceptible to secondary xylem embolism compared to the other two species, but all three maintained hydration of the vascular cambium under severe stress, which could facilitate hydraulic recovery by regrowth of xylem when stress is relieved.

KEY WORDS anatomy; cotyledon; drought; hydraulic capacitance; hypocotyl; *Larix occidentalis*; microCT; *Pinus ponderosa*; *Pseudotsuga menziesii*; xylem embolism.

Extensive first-year seedling mortality, which can be greater than 99% (Cui and Smith, 1991; Johnson and Smith, 2005; Mellmann-Brown, 2005) suggests a life history bottleneck that is fundamentally important to determining rates of recruitment, population persistence, and migration (Haig et al., 1941; Burns and Honkala, 1990; Cui and Smith, 1991; Johnson et al., 2011; Calama et al., 2015; Reinhardt et al., 2015; Clark et al., 2016; Wang et al., 2016; Conlisk et al., 2017; Brodersen et al., 2019). Unlike saplings and adult trees, young seedlings are exposed to dramatic ground-level microclimate variability (Germino and Smith, 1999, 2001; Johnson and Smith, 2005; Maher et al., 2005; Johnson et al., 2011). Young seedlings also cannot access deep water, and they have limited stores of carbohydrates they can use to persist through stressful conditions (Johnson et al., 2011; Reinhardt et al., 2015). Thus, variations in anatomy and physiology throughout development may be particularly important in determining their establishment and success. Because working with small seedlings is difficult, due to their fragility, we lack a fundamental understanding of the hydraulic and biomechanical responses of young seedlings to drought stress (Calama et al., 2015; Larson et al., 2020).

Previous research has illustrated correlations between xylem anatomical traits to resistance to embolism and theoretical maximum hydraulic conductivities (Domec et al., 2006; Pittermann et al., 2006; Choat et al., 2008). Working within this framework, Miller and Johnson (2017) found that during the first 10 weeks of growth of seedlings of *Pseudotsuga menziesii* (Pinaceae), *Pinus ponderosa* (Pinaceae), and *Larix occidentalis* (Pinaceae), seedlings quickly shift from reliance on primary xylem to secondary

xylem, thereby transitioning to a less hydraulically conductive but more embolism-resistant vascular system. Yet, the anatomical analyses did not reveal how the distribution of tracheid sizes and types (primary vs. secondary xylem) might influence changes in conductivity during desiccation. Primary tracheal elements, metaxylem specifically, are larger in diameter, and thus have the potential to be more hydraulically conductive than the narrower secondary tracheids (Tyree and Zimmermann, 2002). As a consequence, primary xylem conduits tend to embolize at less-negative water potentials (Choat et al., 2015, 2016). The age and/or water potential at which this transition occurs is unclear, and sustained water transport may depend on continued function of particular populations of tracheids in very young conifer seedlings. In addition to characterizing xylem-specific traits, Miller and Johnson (2017) also reported large amounts of extraxylary tissue, including numerous lignified axial parenchyma within the vasculature and large proportions of cortical tissue within the stems in addition to the vasculature. Considering the large amounts of extraxylary tissue in these seedling stems compared to their adult counterparts, these tissues might play a role in sustaining conductivity during desiccation (e.g., by providing a source of stored water).

To further expand upon the anatomical analyses by Miller and Johnson (2017), we characterized young seedling hydraulic and anatomical responses to drought. Specifically, we used noninvasive high-resolution x-ray microcomputed tomography (microCT) imaging and concurrent hydraulically measured specific conductivity (k_s) during desiccation to determine the relationships between drought stress and embolism formation in the primary versus secondary xylem during dehydration in young seedlings of *P. menziesii*, *L. occidentalis*, and *P. ponderosa*. We hypothesized that (1) declines in conductivity during desiccation would depend primarily on xylem embolism rather than extraxylary tissue damage, and as such, a strong correlation would be seen between k_s and in planta xylem embolism visualization; (2) primary xylem would embolize under milder stress compared to secondary xylem, and thus, initial declines in k_s would be driven by primary xylem embolism.

MATERIALS AND METHODS

Plant materials and growing conditions

Seeds were initially germinated at the University of Idaho's Franklin H. Pitkin Forest Nursery located in Moscow, Idaho, USA (46°43′N, 116°59′W), then transported to the University of Idaho's Sixth Street Greenhouse. All seeds were locally collected to minimize effects of geographical differences on inter- and intraspecific characteristics. On 20 May 2015, approximately 2-week-old *P. menziesii* var. *glauca* and *L. occidentalis* seedlings were transplanted from styro-growing blocks into 9.1 × 9.1 × 10.8 cm Anderson Pots (AB45; Stuewe & Sons, Tangent, Oregon, USA); *P. ponderosa* var. *ponderosa* was sown directly from seed on the same date. All species were grown for 4 weeks in a commercial potting mix (Metro-Mix Custom Blend, Sun Gro Horticulture, Agawam, MA, USA) consisting of 45% Canadian sphagnum peat moss, 45% vermiculite, and 10% bark. Seedlings were shipped overnight from Moscow, Idaho to Berkeley, California 1 day before microCT imaging.

On the day of imaging, seedlings were removed from their shipping containers and either kept in the dark or placed under a bright work light and a fan. Seedlings were allowed to dry down under these conditions for approximately 24 h. Once we realized that the seedlings were not going to get as dry as desired for the experiment, a subset was excised at the root collar to expedite drying (see below). Ranges of water potentials measured for excised and intact seedlings was −0.1 to −6.73 and approximately −0.01 to −4.32 MPa, respectively (see below for measurement details).

X-ray computed microtomography (microCT)

In planta responses to desiccation were imaged utilizing high-resolution x-ray microCT (Beamline 8.3.2; Advanced Light Source, Berkeley, CA, USA). MicroCT allows for non-invasive visualization of gas-filled spaces (dark gray) versus hydrated live cells and water-filled functional xylem (light gray) (Fig. 1). Due to the numerous different tissues in the seedling stems and substantial changes during growth, microCT images were compared to confocal laser scanning microscopy images of the same species and ages to assist with tissue identification, and in some cases, anatomical quantification (Fig. 1; see Stem desiccation and xylem embolism quantification section below). Eighty seedlings (either as intact seedlings or excised stems) were scanned between the root collar and the crown base: 16, 19, and 15 intact seedlings (not cut before imaging) of *P. ponderosa*, *P. menziesii*, and *L. occidentalis*, respectively, and 10 excised stems per species were scanned (see next section). We used 6-week-old *P. menziesii* seedlings (stems were ca. 40 mm from root collar to base of crown, 0.85 ± 0.03 [SE] mm mid-stem diameter), 6-week-old *L. occidentalis* seedlings (19 mm length and 0.73 ± 0.03 mm mid-stem diameter), and 4-week old *P. ponderosa* seedlings (37 mm length and 1.34 ± 0.03 mm mid-stem diameter) for the measurements described below. Four-week-old *P. ponderosa* seedlings were used because 6-week-old *P. ponderosa* seedlings would have been too large for microCT imaging.

All microCT imaging was performed using the methods of McElrone et al. (2013). Seedlings or stems were mounted on a custom holder, covered by an acrylic cylinder to dampen vibration, and positioned on the sample stage. Samples were imaged at 24 keV while the sample was rotated 180° through the x-ray beam. Images were captured by a camera (PCO EDGE; Cooke Corp., Romulus, MI, USA) with a 5× magnification long working distance objective lens (Mitutoyo Corp., Kawasaki, Japan). The raw projection images were then reconstructed using a custom ImageJ plugin (Institute for Nuclear Sciences, University of Ghent, Belgium). The reconstructed images had a voxel size of 1.338 × 1.338 × 1.338 µm (*x*, *y*, *z* pixel dimensions). Each sample (intact seedling or excised stem) was imaged once. Immediately after imaging, both intact seedlings (stem cut in 20 mM aqueous KCl) and excised stems were labeled and placed in a 20 mM aqueous KCl. Hydraulic conductivity and water potential measurements were then

FIGURE 1. Confocal micrographs (A, C, E) and computed microtomographic images (B, D, F) for *Larix occidentalis* (A, B), *Pseudotsuga menziesii* (C, D), and *Pinus ponderosa* (E, F) with anatomical components labeled. ep = epidermis, mx = metaxylem, P = pith, pc = primary cortex, pe = periderm, ph = phloem, px = protoxylem, rc = resin canal, sx = secondary xylem, vc = vascular cambium zone. Red arrows indicate gas-filled intercellular spaces, in these specific cases, within the cortex and pith regions. Bars = 100 µm. Confocal micrographs were either modified by permission from Miller and Johnson (2017) or were imaged as described therein.

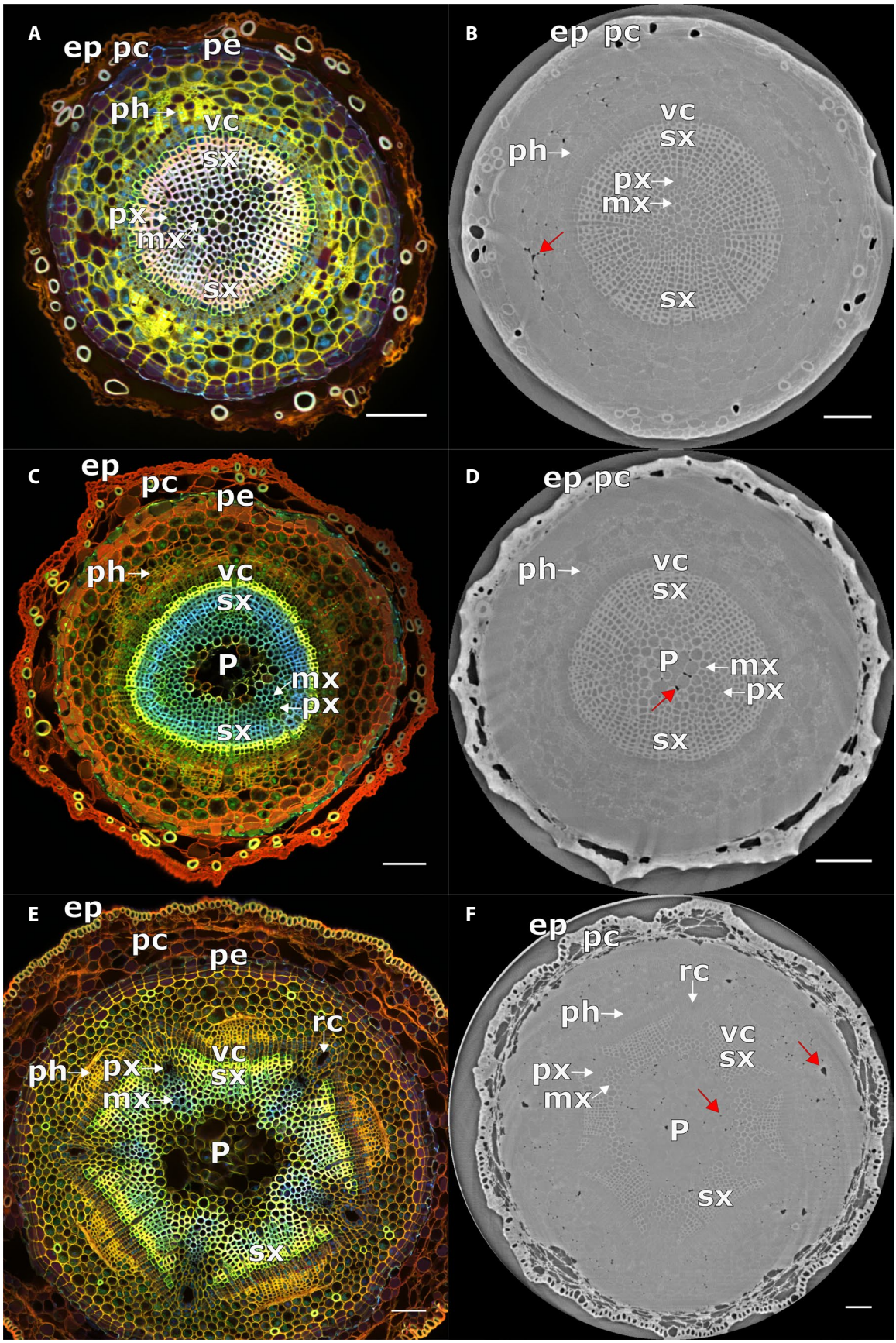
A
ep
pc
pe
ph
vc
sx
px
mx
sx
B
ep
pc
vc
sx
ph
px
mx
sx
C
ep
pc
pe
ph
vc
sx
P
mx
px
sx
D
ep
pc
ph
vc
sx
P
mx
px
sx
E
ep
pc
pe
rc
ph
px
vc
sx
mx
P
sx
F
ep
pc
rc
ph
vc
sx
px
mx
P
sx

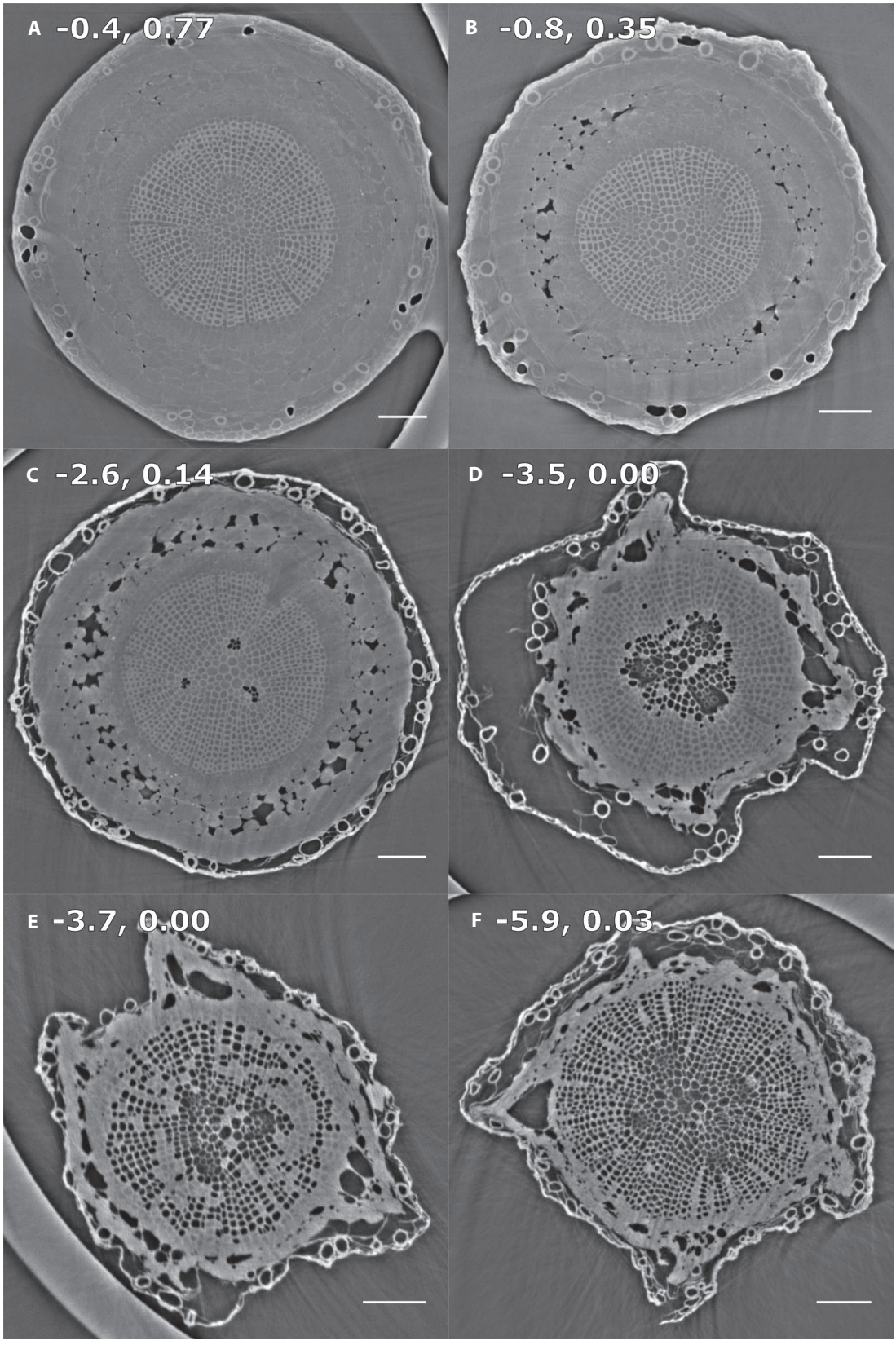

FIGURE 2. Pattern of desiccation for (A–F) *Larix occidentalis*. Numbers adjacent to box letters indicate measured water potential in MPa; numbers following water potentials indicate specific hydraulic conductivity of the imaged stem in kg m^{-1} s^{-1} MPa^{-1}.

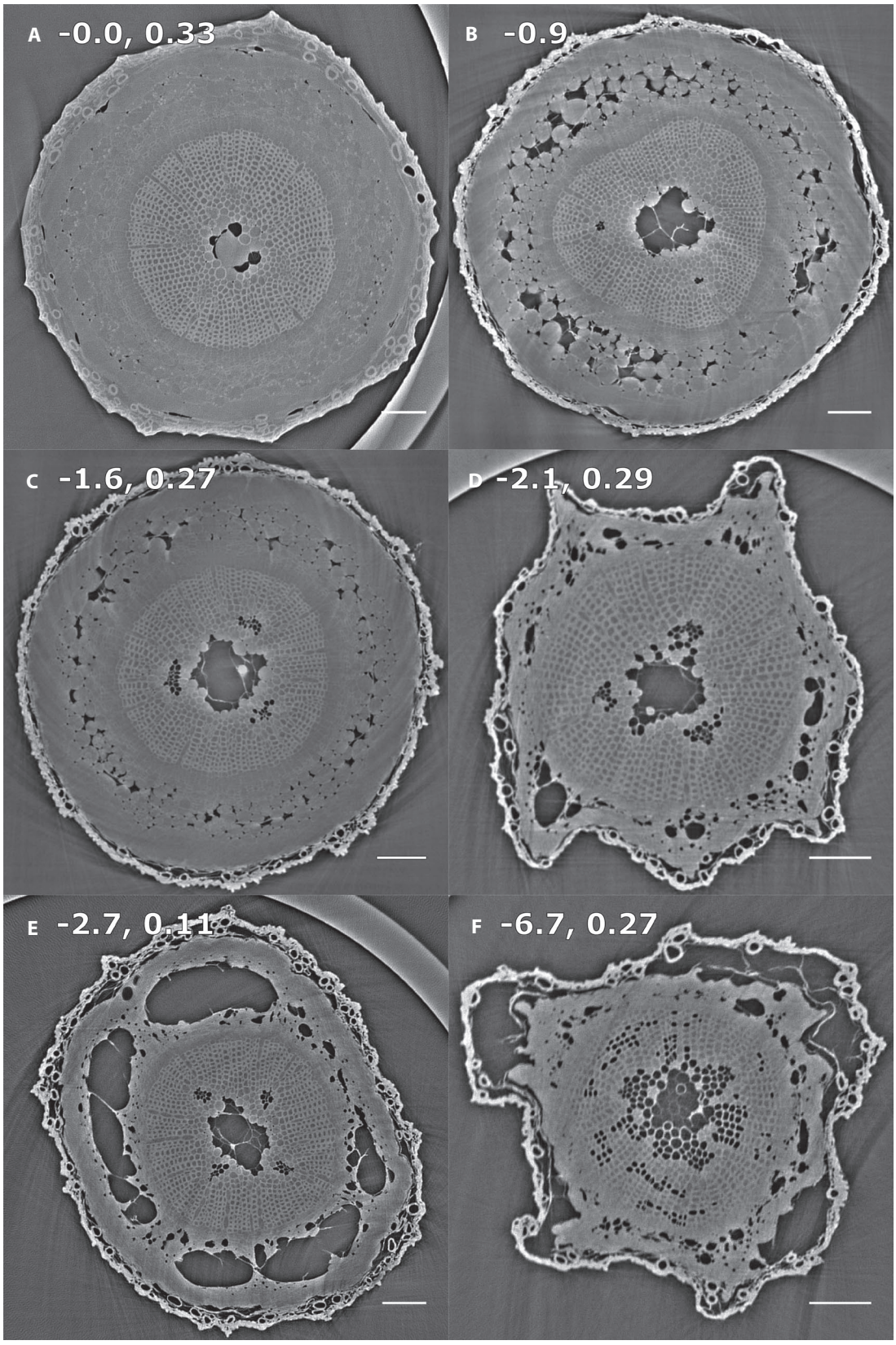

FIGURE 3. Pattern of desiccation for (A–F) *Pseudotsuga menziesii*. Numbers adjacent to box letters indicate measured water potential in MPa; numbers following water potentials indicate specific hydraulic conductivity of the imaged stem in kg m^{-1} s^{-1} MPa^{-1} (panels without conductivity measurements indicate imaged stems that did not have associated conductivity measurements).

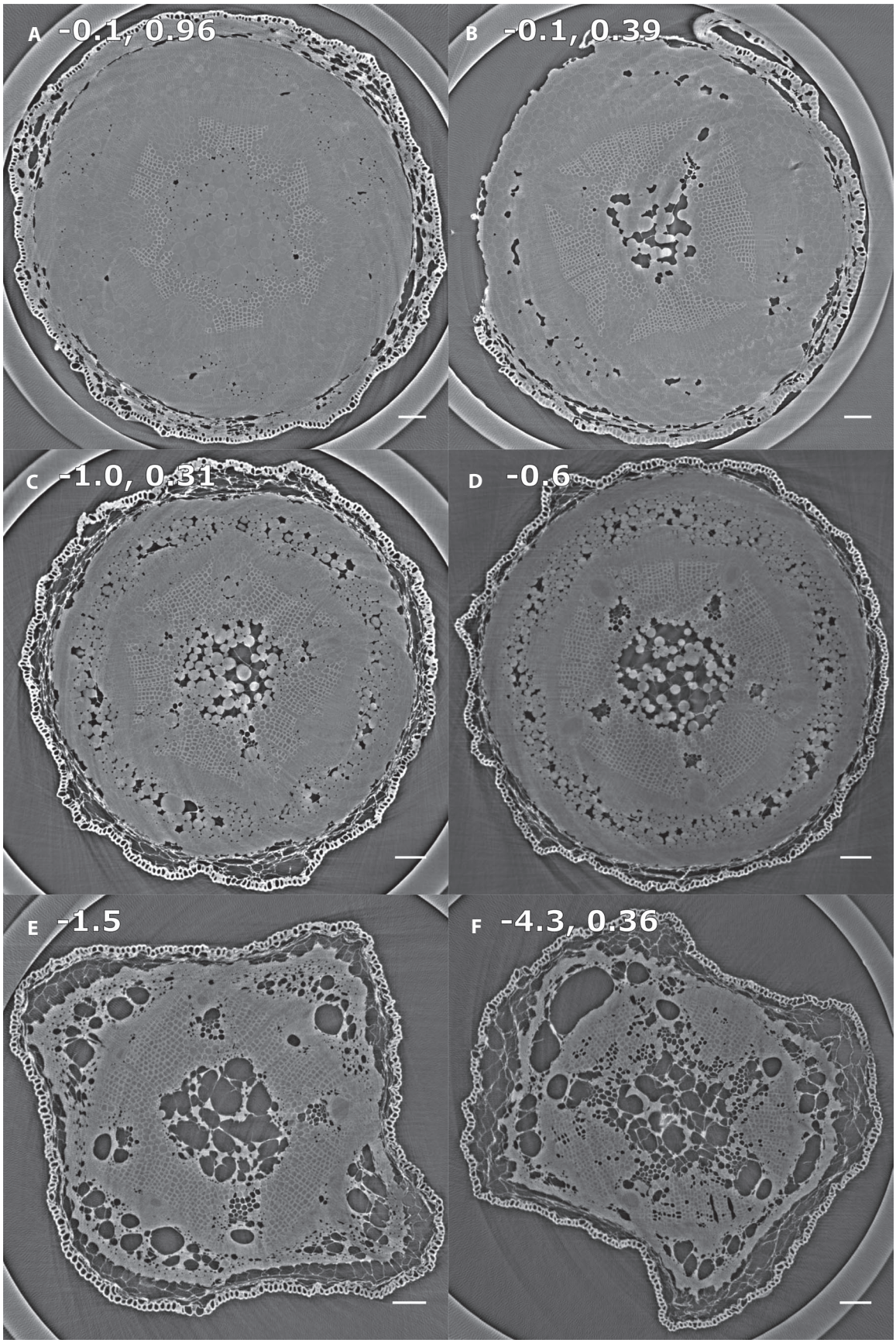
A -0.1, 0.96
B -0.1, 0.39
C -1.0, 0.31
D -0.6
E -1.5
F -4.3, 0.36

FIGURE 4. Pattern of desiccation for (A–F) *Pinus ponderosa*. Numbers adjacent to box letters indicate measured water potential in MPa; numbers following water potentials indicate specific hydraulic conductivity of the imaged stem in kg m^{-1} s^{-1} MPa^{-1} (panels without conductivity measurements indicate imaged stems that did not have associated conductivity measurements).

started on all stems (from both previously intact seedlings and stems that had been previously excised).

Hydraulic conductivity, water potential, and vulnerability to hydraulic dysfunction

Excised stems from both previously intact and previously excised samples were placed in degassed, filtered, 20 mM aqueous KCl under a partial vacuum overnight. Two stems per species were removed from the vacuum solution, immediately microCT-imaged, and subsequently measured for maximum k_s; the remainder of the excised stems were bench-dehydrated. Periodically during the dry down, stem segments were selected at random and then imaged, then immediately measured for k_s and water potential, with the last stem imaged and measured ca. 16 h after the start of the bench dehydration. Hydraulic conductivity and water potential were measured once for each stem.

We used a modified Sperry apparatus (Sperry et al., 1988) to measure stem hydraulic conductance (k_h). One end of the stem segment was connected to an upstream reservoir containing filtered, degassed 20 mM aqueous KCl via an inline low flow meter (Sensirion SLI-0430, Stafa, Switzerland). The other end of the stem segment was placed directly into a shallow water reservoir (downstream) to prevent flow variability due to droplet accumulation and release as water flowed out of the stem. This modified method required only one side of the stem to undergo physical manipulation, which reduced the potential for mechanical damage and leaks at the stem-to-tube connection points in these small and delicate stem samples. Hydraulic conductance (k_h) was calculated as the stabilized (~5–10 min) output of the flowmeter (volume/time) divided by the pressure gradient created by the difference in height between upstream and downstream water reservoirs. Hydraulic conductance was then normalized by the length and stem cross-sectional area of the sample, calculated from the average of four diameter measurements per stem, for stem specific conductivity (k_s) (Sperry et al., 1988; Tyree and Zimmermann, 2002). The length of stems used in the conductivity measurements was 3.0 (SE = 0.2) cm, 2.9 (SE = 0.1) cm and 1.8 (SE = 0.1) cm for *P. ponderosa*, *P. menziesii*, and *L. occidentalis*, respectively. Nonlignified tissues (i.e., extraxylary tissues) were not removed from the stem before conductivity measurements due to the small diameters of the samples.

Screen-cage thermocouple psychrometers (Merrill Specialty Equipment, Logan, UT, USA) were used to measure water potential () on equilibrated leaf tissue in the case of seedlings with intact stems or small stem segments in the case of excised stems. Before the experiment, the psychrometers were calibrated with four different NaCl solutions spanning the range of 0 to −7 MPa based on the relationship between NaCl concentration and water potential (Brown and Bartos, 1982). Samples were enclosed in stainless steel psychrometer chambers, triple-bagged, submerged in a 25°C water bath, and equilibrated for at least 4 h or until sequential measurements were stable. Psychrometer measurements were recorded by an AM16/32B multiplexer interfaced to a CR6 data logger (Campbell Scientific, Logan, UT, USA). Hydraulic vulnerability curves for each species were expressed as k_s as a function of Ψ with intact and excised stem measurements pooled. Each point on the graph generated from these data represents a different individual seedling.

Stem desiccation and xylem embolism quantification

Stem cross-sectional diameters, xylem cross-sectional diameters, total xylem area, and stem core diameters (effectively measuring the diameter of the stem excluding the epidermis and remnant crushed primary undifferentiated cortex outside of the periderm; Fig. 1)

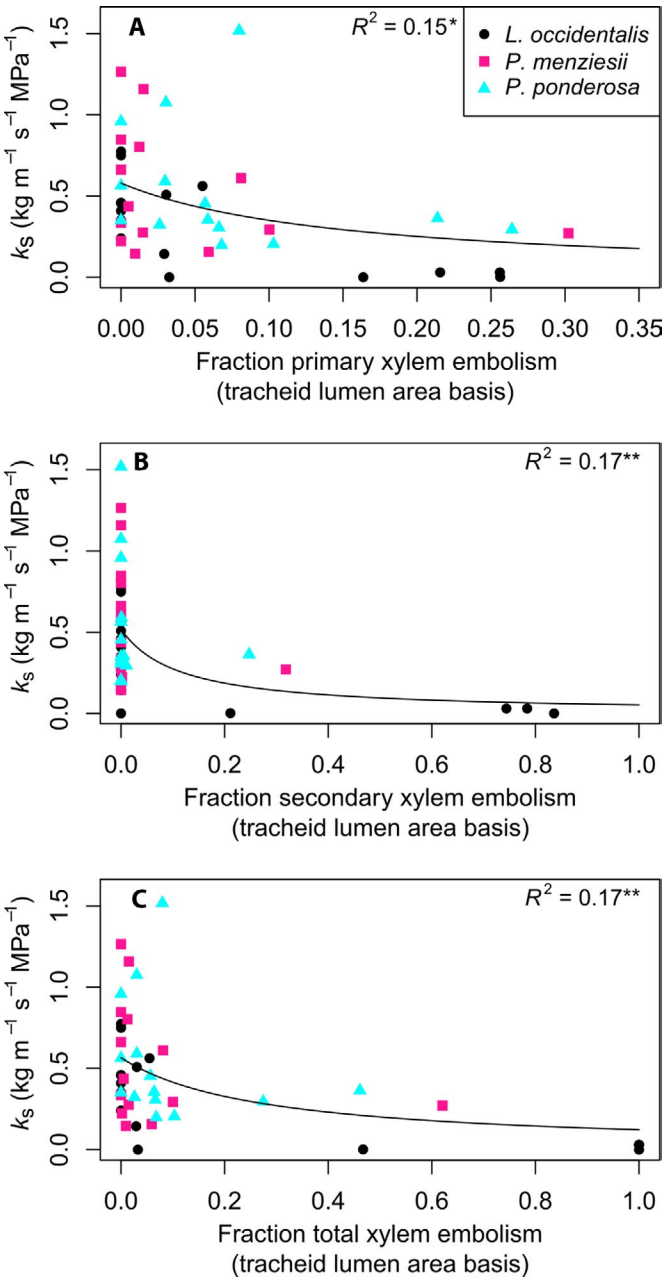

FIGURE 5. Response of conductivity broken down between tissues: (A) primary xylem embolism, (B) secondary xylem embolism, and (C) total xylem embolism. Significance of R^2: **0.001 ≤ P < 0.01 and * 0.01 ≤ P < 0.05.

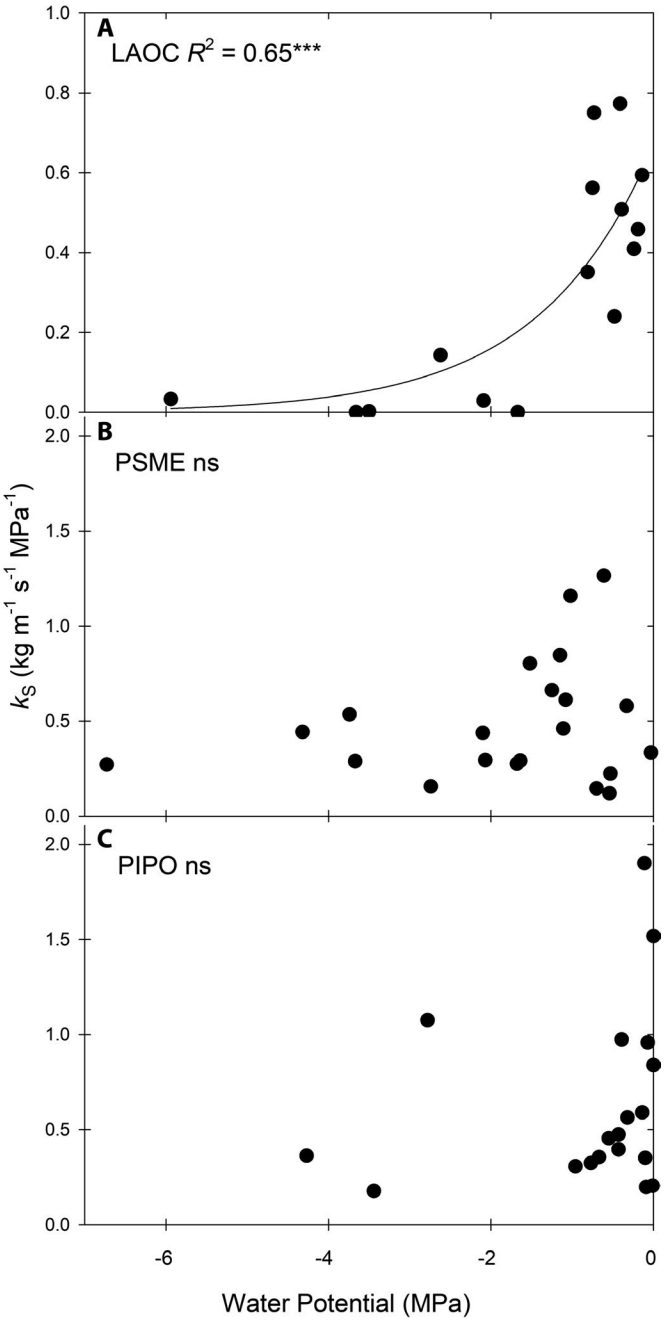

FIGURE 6. Response of k_s to decreasing ψ for (A) *Larix occidentalis*, (B) *Pseudotsuga menziesii*, and (C) *Pinus ponderosa*. Each dot respresents an individual seedling. Although general trends include exponential-decay shaped curves, significant curve fits could not be obtained for *P. menziesii* and *P. ponderosa*. These graphs illustrate the large intra-specific variability possible between individuals within a population, especially within *P. menziesii*. Significance of R^2: *** $P < 0.001$.

were measured directly from the microCT images using ImageJ (Schindelin et al., 2012; Schneider et al., 2012; Rueden et al., 2017). Stem and xylem cross-sectional areas were calculated from diameter measurements; in the case of stems that were severely warped due to dehydration, stem and cortex areas were measured directly with ImageJ using hand drawn tools.

Xylem embolism and extraxylary air-filled voids were quantified from microCT images for most stems that had been measured for both k_s and Ψ (several microCT scans were not in focus enough to analyze). Actual embolized lumen and air void areas were measured using a semi-automated thresholding of air-filled spaces followed by hand corrections using the magic wand tool in Fiji/ImageJ. Embolized lumen were classified into primary and secondary xylem.

To calculate percentage embolism of the xylem, estimates of functional xylem lumen area were necessary. Previous analyses on identically aged seedling stems of each species (Miller and Johnson, 2017) illustrated that a large portion of the lignified cells within the vascular bundle were axial parenchyma rather than mature tracheal elements and thus likely nonfunctional in axial water transport; microCT image analyses were not able to distinguish between the parenchyma cell contents and water-filled tracheids. Therefore, to estimate tracheid-specific xylem characteristics, the raw data from Miller and Johnson (2017) were used to generate species-specific estimates of total lumen area (which included tracheid and parenchyma lumen area), functional xylem area (which included tracheid lumen and cell wall tissue), and total tracheal lumen area (tracheid lumen area only). Unless otherwise stated, estimates of xylem embolism are expressed on total xylem area basis.

Statistical analyses

Statistical analyses were conducted in R Studio (V.1.0.143 running R versions V.3.4.0–V.3.4.3; RStudio Boston, MA, USA). Hydraulic conductivity was modeled as a function of primary xylem embolism, secondary xylem embolism, lacunae, total xylem embolism (incorporating primary xylem embolism) and total stem air fraction (incorporating all three main tissues). Xylem and extraxylary influences on k_s were modeled with both nonlinear and linear regression; variables were translated and transformed as necessary to meet linear modeling assumptions. To explicitly test hypothesis 2, we developed a model with k_s as a function of (water potential × primary xylem embolism) + (water potential × secondary xylem embolism). Additionally, we ran two simpler models with primary xylem embolism as a function of water potential and secondary xylem embolism as a function of water potential.

We utilized a combination of the ncvTest in the car package and diagnostic plots to evaluate the heteroscedasticity of the linear models. When transformations did not fulfill linear modeling assumptions of homoscedasticity, a heteroscedasticity-corrected coefficient covariance matrix was applied (Anova type III, white.adjust = TRUE, car package; Fox and Weisberg, 2011; Long and Ervin, 2000), which modified standard errors and p-values accordingly; R^2 values were not available for heteroscedastic-corrected models.

All nonlinear curve fits were performed using SigmaPlot (V. 12.0, SPSS, San Rafael, CA, USA). Parameters were added in a forward selection process, and best-fit models were selected based on adjusted R^2 values.

RESULTS

Tissue desiccation and damage

Similar patterns of stem desiccation were observed for all three species (Figs. 2–4, see also Fig. 5 and Appendix S1). Initial water

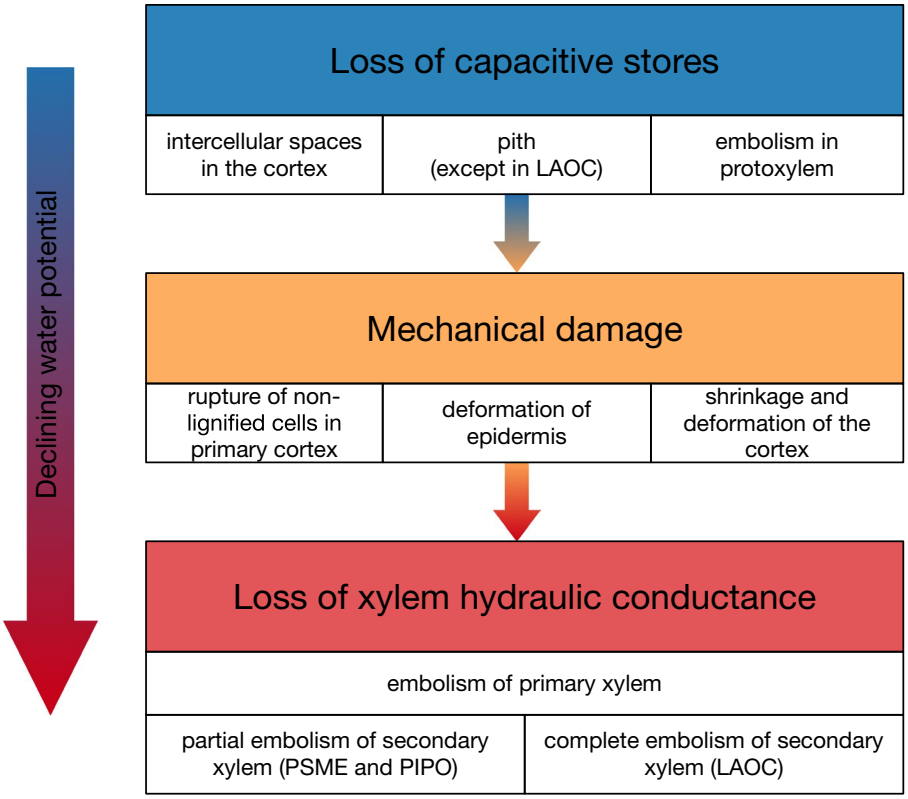

FIGURE 7. Schematic diagram detailing observed patterns during seedling dehydration.

depletion (at the least-negative water potentials) occurred first within the intercellular spaces in the cortex and the pith and occasionally within the protoxylem of the well-watered, intact seedlings. Initial cortical airspaces/voids occurred between the developing periderm and the phloem, while the pith voids occurred between individual parenchyma or xylem cells. Continued dehydration resulted in the expansion of cortical and pith air void areas and embolism of the protoxylem clusters (if not previously embolized), followed by progressive embolism of the metaxylem across all species.

Additional desiccation resulted in embolism of the remaining primary xylem and severe tissue damage to the cortex and epidermal tissues. In some cases, the vascular cylinder became completely uncoupled from the epidermis (Figs. 2D, 3F, 4E). Substantial secondary xylem embolism occurred only at the most-severe water stress levels across all species (Figs. 2E, 2F, 3F, 4F). All species experienced statistically significant shrinkage of cross-sectional stem areas during desiccation (*L. occidentalis*: $F_{1, 16} = 4.87$, $p = 0.04$, *P. menziesii*: $F_{1, 16} = 8.84$, $p = 0.009$, *P. ponderosa*: $F_{1, 13} = 10.81$, $p = 0.006$), while changes in xylem area were non-significant (data not shown, but see xylem areas in Figs. 2–4). However, even at the most-negative water potentials, the vascular cambium remained hydrated in all three species.

Even in the well-hydrated stems, there were some gas-filled spaces within the pith and cortex (Figs. 2A, 3A, 4A). Extensive air void expansion and extraxylary tissue damage occurred throughout the dry-down period (Fig. 5; Appendix S2). Air voids in the cortex and pith and primary xylem embolism accounted for the majority of air-filled spaces during desiccation. Primary xylem embolism was observed at relatively mild water potentials (>–1 MPa) in all species. However, secondary xylem was much more resistant to embolism and was observed only at water potentials more negative than –2 MPa. The secondary xylem in *L. occidentalis* was nearly completely embolized at the most negative water potentials. However, secondary xylem in *P. ponderosa* and *P. menziesii* remained mostly water-filled even at the most-negative water potentials.

While primary xylem contributed almost exclusively to total xylem embolism above –3 MPa, secondary xylem contributed equal amounts or a greater proportion of total xylem embolism in all stems below than –3 MPa (Fig. 5). There were no instances where secondary xylem embolism occurred at water potentials less negative than primary xylem embolism. At the most-negative water potentials, *P. ponderosa* and *P. menziesii* exhibited maximum secondary xylem embolism of 24.7% and 31.8%, respectively (at water potentials of –4.3 and –6.7 MPa) for a total of 47.7% and 62.1% total xylem embolism, respectively (Fig. 5). *Larix occidentalis* on the other hand, exhibited 78% xylem embolism at its most-negative water potential (–5.9 MPa). Calculations of embolism expressed on a total lumen area (as opposed to tracheid lumen area; data not shown) indicated that 85–100% of axial parenchyma plasmolyzed in the three individuals with the lowest water potentials, which ranged from –2.1 to –5.9 MPa (Fig. 2D, E).

Hydraulic conductivity responses to desiccation

Although only *L. occidentalis* exhibited a significant relationship between water potential and k_s (Fig. 6), there were visual trends in declining k_s with decreasing water potential in both *P. menziesii* and *P. ponderosa* (see Discussion). However, in contrast to *L. occidentalis*, neither *P. menziesii* nor *P. ponderosa* reached zero k_s at the most-negative water potentials, which was corroborated by the microCT images across these species (i.e., secondary xylem not highly embolized). Both primary and secondary xylem embolism contributed to k_s decline: total xylem embolism and secondary xylem embolism were the strongest predictors of k_s across all species based on individual variable comparisons (Fig. 5), but all tissue types including cortical air voids had significant relationships with k_s but with weak explanatory power ($R^2 = 0.14 – 0.17$; Fig. 5). However, due to large amounts of variability, our original hypothesis that primary xylem embolism would have the largest impact on hydraulic conductivity (as compared to secondary xylem) was not statistically supported.

DISCUSSION

Very young seedlings must be able to tolerate drought as early as within the first month post-germination (Haiget al., 1941) in

places like the northwestern United States, which is characterized by seasonal summer droughts. Research to date is sparse regarding first-year seedling hydraulic properties and drought-induced dysfunction (Zavitkovski and Ferrell, 1968; Brix, 1979; Cui and Smith, 1991; Kolb and Robberecht, 1996; Maherali et al., 2002; Abatzoglou et al., 2014; Reinhardt et al., 2015). However, the little information that is available demonstrates that seedling vulnerability cannot be extrapolated from their adult counterparts (e.g., Cui and Smith, 1991; Urli et al., 2013). Additionally, the differences in fundamental anatomy between emergent seedling stems and sapling or mature stems and branches seem to suggest that biomechanical responses will necessarily be different as well; thus, the complex interactions of primary xylem and air voids outside the xylem add elements to seedling hydraulic functionality that are, as of yet, unexplored.

Cell shrinkage and air expansion in pith and cortex

Air void expansion, a result of cell shrinkage, in the pith and cortex began at very mild water potentials (>−1 MPa) and continued throughout the desiccation process until large areas of the stem were air-filled (Figs. 2–5). It is possible that the water that was contained in these areas during full hydration served as a capacitive store and was released into the transpiration stream to maintain secondary xylem function (see Fig. 7). Brodersen and Pittermann (2016) found similar patterns of cellular collapse within the cortex and around the vascular tissue of fern stipes during desiccation, as well as highly resistant xylem conduits using similar methods. It is therefore noteworthy that the cortex may be playing a functionally similar role in two divergent groups (i.e., ferns and conifers) before the formation of woody tissue in the seedling stage.

Primary and secondary xylem embolism

Primary xylem embolism occurred in all species at relatively mild water potentials and may have driven initial declines in conductivity. Although this relationship was not supported statistically, the large amount of variation in individual seedling k_s (see Fig. 5) likely obscured potential relationships between primary xylem embolism and conductivity. Choat et al. (2015) also observed empty primary xylem at mild water potentials in saplings of *Sequoia sempervirens*. Primary xylem embolism in the current study could also serve as another source of capacitive water preventing dysfunction of the secondary xylem. Secondary xylem embolism only occurred at the most-negative water potentials and was associated with a k_s of zero in *L. occidentalis*. In the other two species, secondary xylem never completely embolized, and flows were still measurable even at the most-negative water potentials. However, even in *P. ponderosa* and *P. menziesii*, k_s at highly negative water potentials (<−4 MPa) was only 10 to 20% of maximum values measured at full hydration. Few data exist on the water potentials of young conifer seedlings in their natural environments, but water potentials of approximately −3 MPa appeared to represent a mortality threshold in *P. ponderosa* first year seedlings in multiple studies (Simeone et al., 2018; Augustine and Reinhardt, 2019). Based on data presented here and data of Simeone et al. (2018), *P. ponderosa* seedlings at −3 MPa would have had the majority of their stem xylem hydraulic capacity intact.

As the seedling cortex and epidermis were becoming distorted and mechanical damage was occurring during dehydration (e.g., see Fig. 3E, F), the secondary xylem and the vascular cambium remained mostly hydrated in *P. ponderosa* and *P. menziesii*. Even in *L. occidentalis*, which experienced large amount of secondary xylem embolism, the vascular cambium remained hydrated even at very negative water potentials (Fig. 2E, F). The maintenance of cambium hydration suggests that these seedlings have some ability to recover from drought and to make new xylem and phloem if carbon stores are available.

Sources of variation and moving forward

One limitation of the current study is the variation in k_s measurements. This variation could be due to measurement error; flows were very low through these small samples (most were less than 1 mm in diameter). Additionally, there could have been errors in the psychrometric measurements due to the small amount of tissue in the chambers. The next steps would be to establish mortality thresholds for species-age specific emergent seedlings and link biomechanical changes and in planta embolism to mortality thresholds (see Simeone et al., 2018 and Sapes et al., 2019). Additionally, maintenance of xylary transport in *P. menziesii* and *P. ponderosa* down to ca. −4 and −6 MPa, respectively, indicate that these seedlings may be able to transport some water even in extreme circumstances and that seedling mortality may not be a direct result of loss of the stem water transportation network, but instead may be attributed to other dysfunction, such as hydraulic failure in the rhizosphere (Johnson et al., 2018). Though the phloem was not specifically analyzed here, microCT images indicate likely disruption to the phloem via air void expansion and stem deformation, and possible disruption to the vascular cambium. Although, in some cases, the vascular cambium appears intact despite extensive cortical damage (e.g., Fig. 2E). Thus, future seedling research should also assess the viability of the cells surrounding the lignified vascular region during desiccation to evaluate permanent cell death and possible recovery.

ACKNOWLEDGMENTS

This work was supported by the National Science Foundation (grant nos. IOS-1146746 and 1852976) and University of Idaho C.R. Stillinger Forest Science Research Fellowship. The Advanced Light Source is supported by the Director, Office of Science, Office of Basic Energy Science, of the U.S. Department of Energy under contract no. DE-AC02-05CH11231. We thank Dula Parkinson and Parker Holden at the Advanced Light Source for beamline and image reconstruction support, Drs. David Tank and Blair McLoughlin for comments on the manuscript, and Karl Meyer for his assistance in microCT image analysis. We also thank two anonymous reviewers for their comments which resulted in an improved paper. A.J.M. was supported by the USDA CRIS Project No. 2032-21220-006-00D.

DATA AVAILABILITY

All hydraulic and anatomical analysis data are available from the Dryad Digital Repository: https://doi.org/10.5061/dryad.kkwh70s2c (Miller et al., 2020).

SUPPORTING INFORMATION

Additional Supporting Information may be found online in the supporting information tab for this article.

APPENDIX S1. Air-filled voids (A) and xylem embolism (B, C) in stems during dehydration.

APPENDIX S2. Response of conductivity broken down between tissues (A–C), total xylem embolism (D), and total stem air, including lacunae and xylem embolism (E). Although k_s trends downward with primary xylem embolism (A), there are still numerous individuals across all species with zero primary xylem embolism. Secondary xylem embolism appears to have almost no influence on k_s until greater than 20% embolism is reached (B), which corresponded to ca. −3 MPa. Expansion of lacunae appears to account for a smaller amount of variability compared with either xylem type as indicated by the R^2 value (C). Total xylem embolism is represented in (D) and total core air fraction in (E). Results based on R^2 values indicate that total xylem embolism accounts for the most variability in k_s, meaning it is the best predictor of k_s of those tested. However, the small R^2 values, though significant, strongly indicated that there are other significant variables not taken into account. Significance of R^2 is annotated as $^{***}P < 0.001$, $^{**}0.001 \leq P < 0.01$, $^{*}\ 0.01 \leq P < 0.05$.

LITERATURE CITED

Abatzoglou, J. T., D. E. Rupp, and P. W. Mote. 2014. Seasonal climate variability and change in the Pacific Northwest of the United States. *Journal of Climate* 27: 2125–2142.

Augustine, S. P., and K. Reinhardt. 2019. Differences in morphological and physiological plasticity in two species of first-year conifer seedlings exposed to drought result in distinct survivorship patterns. *Tree Physiology* 39: 1446–1460.

Brix, H. 1979. Effects of plant water stress on photosynthesis and survival of four conifers. *Canadian Journal of Forest Research* 9: 160–165.

Brodersen, C. R., M. J. Germino, D. M. Johnson, K. Reinhardt, W. K. Smith, L. M. Resler, M. Bader, A. Sala, et al. 2019. Seedling survival at timberlines is critical to conifer mountain forest elevation and extent. *Frontiers in Forests and Global Change* 2: 9.

Brodersen, C. R., C. Rico, O. Guenni, and J. Pittermann. 2016. Embolism spread in the primary xylem of *Polystichum munitum*: implications for water transport during seasonal drought. *Plant, Cell and Environment* 39: 338–346.

Brown, R. W., and D. L. Bartos. 1982. A calibration model for screen-caged Peltier thermocouple psychrometers. U.S. Department of Agriculture, Forest Service, Intermountain Forest and Range Experiment Station, Ogden, UT, USA.

Burns, R. M., and B. H. Honkala. 1990. Silvics of North America, Agricultural Handbook 654. U. S. Department of Agriculture, Washington, D.C., USA.

Calama, R., J. Puértolas, R. Manso, and M. Pardos. 2015. Defining the optimal regeneration niche for *Pinus pinea* L. through physiology-based models for seedling survival and carbon assimilation. *Trees-Structure and Function* 29: 1761–1771.

Choat, B., E. Badel, R. Burlett, S. Delzon, H. Cochard, and S. Jansen. 2016. Noninvasive measurement of vulnerability to drought-induced embolism by x-ray microtomography. *Plant Physiology* 170: 273.

Choat, B., C. R. Brodersen, and A. J. McElrone. 2015. Synchrotron x-ray microtomography of xylem embolism in *Sequoia sempervirens* saplings during cycles of drought and recovery. *New Phytologist* 205: 1095–1105.

Choat, B., A. R. Cobb, and S. Jansen. 2008. Structure and function of bordered pits: new discoveries and impacts on whole-plant hydraulic function. *New Phytologist* 177: 608–626.

Clark, J. S., L. Iverson, C. W. Woodall, C. D. Allen, D. M. Bell, D. C. Bragg, A. W. Amato, et al. 2016. The impacts of increasing drought on forest dynamics, structure, and biodiversity in the United States. *Global Change Biology* 22: 2329–2352.

Conlisk, E., C. Castanha, M. J. Germino, T. T. Veblen, J. M. Smith, and L. M. Kueppers. 2017. Declines in low-elevation subalpine tree populations outpace growth in high-elevation populations with warming. *Journal of Ecology* 105: 1347–1357.

Cui, M., and W. K. Smith. 1991. Photosynthesis, water relations and mortality in *Abies lasiocarpa* seedlings during natural establishment. *Tree Physiology* 8: 37–46.

Domec, J. C., B. Lachenbruch, and F. C. Meinzer. 2006. Bordered pit structure and function determine spatial patterns of air-seeding thresholds in xylem of Douglas-fir (*Pseudotsuga menziesii*; Pinaceae) trees. *American Journal of Botany* 93: 1588–1600.

Fox, J., and S. Weisberg. 2011. An R companion to applied regression, 2nd ed. SAGE, Los Angeles, CA, USA.

Germino, M. J., and W. K. Smith. 1999. Sky exposure, crown architecture, and low-temperature photoinhibition in conifer seedlings at alpine treeline. *Plant, Cell & Environment* 22: 407–415.

Germino, M. J., and W. K. Smith. 2001. Relative importance of microhabitat, plant form and photosynthetic physiology to carbon gain in two alpine herbs. *Functional Ecology* 15: 243–251.

Haig, I. T., K. P. Davis, and R. H. Weidman. 1941. Natural regeneration in the western white pine type. Northern Rocky Mountain Forest and Range Experiment Station, Missoula, MT, USA.

Johnson, D. M., and W. K. Smith. 2005. Refugial forests of the southern Appalachians: photosynthesis and survival in current-year *Abies fraseri* seedlings. *Tree Physiology* 25: 1379.

Johnson, D. M., K. A. McCulloh, and K. Reinhardt. 2011. The earliest stages of tree growth: development, physiology and impacts of microclimate. *In* F. C. Meinzer, B. Lachenbruch, and T. E. Dawson, [eds.], Tree physiology series, vol. 4, Size- and age-related changes in tree structure and function, 65–87. Springer, Dordrecht, Netherlands.

Johnson, D. M., J.-C. Domec, Z. C. Berry, A. M. Schwantes, D. R. Woodruff, K. A. McCulloh, H. W. Polley, et al. 2018. Co-occurring woody species have diverse hydraulic strategies and mortality rates during an extreme drought. *Plant, Cell and Environment* 41: 576–588.

Kolb, P. F., and R. Robberecht. 1996. *Pinus ponderosa* seedling establishment and the influence of competition with the bunchgrass *Agropyron spicatum*. *International Journal of Plant Sciences* 157: 509–515.

Larson, J. E., B. L. Anacker, S. Wanous, and J. L. Funk. 2020. Ecological strategies begin at germination: traits, plasticity, and survival in the first four days of plant life. *Functional Ecology* 34: 968–979.

Long, J. S., and L. H. Ervin. 2000. Using heteroscedasticity consistent standard errors in the linear regression model. *American Statistician* 54: 217–224.

Maher, E. L., M. J. Germino, and N. J. Hasselquist. 2005. Interactive effects of tree and herb cover on survivorship, physiology, and microclimate of conifer seedlings at the alpine tree-line ecotone. *Canadian Journal of Forest Research* 35: 567–574.

Maherali, H., B. L. Williams, K. N. Paige, and E. H. Delucia. 2002. Hydraulic differentiation of ponderosa pine populations along a climate gradient is not associated with ecotypic divergence. *Functional Ecology* 16: 510–521.

McElrone, A. J., B. Choat, D. Y. Parkinson, A. A. MacDowell, and C. R. Brodersen. 2013. Using high resolution computed tomography to visualize the three dimensional structure and function of plant vasculature. *Journal of Visualized Experiments JoVE* 74: 50162.

Mellmann-Brown, S. 2005. Regeneration of whitebark pine in the timberline ecotone of the Beartooth Plateau, USA: spatial distribution and responsible agents. *In* G. Broll and B. Keplin, [eds.], Mountain ecosystems, 97–115. Springer, Berlin, Germany.

Miller, M. L., and D. M. Johnson. 2017. Vascular development in very young conifer seedlings: theoretical hydraulic capacities and potential resistance to embolism. *American Journal of Botany* 104: 979–992.

Miller, M. L., A. B. Roddy, C. R. Brodersen, A. J. McElrone, and D. M. Johnson. 2020. Anatomical and hydraulic responses to desiccation in emergent conifer

seedlings. *Dryad Digital Repository*. https://doi.org/10.5061/dryad.kkwh70s2c.

Pittermann, J., J. S. Sperry, U. G. Hacke, J. K. Wheeler, and E. H. Sikkema. 2006. Inter-tracheid pitting and the hydraulic efficiency of conifer wood: the role of tracheid allometry and cavitation protection. *American Journal of Botany* 93: 1265–1273.

Reinhardt, K., M. J. Germino, L. M. Kueppers, J.-C. Domec, J. Mitton, and M. Ryan. 2015. Linking carbon and water relations to drought-induced mortality in *Pinus flexilis* seedlings. *Tree Physiology* 35: 771–782.

Rueden, C. T., J. Schindelin, M. C. Hiner, B. E. Dezonia, A. E. Walter, E. T. Arena, and K. W. Eliceiri. 2017. Image J2: ImageJ for the next generation of scientific image data. *BMC Bioinformatics* 18: 529.

Sapes, G., B. Roskilly, S. Dobrowski, M. Maneta, W. R. L. Anderegg, J. Martinez-Vilalta, and A. Sala. 2019. Plant water content integrates hydraulics and carbon depletion to predict drought-induced seedling mortality. *Tree Physiology* 39: 1300–1312.

Schindelin, J., I. Arganda-Carreras, E. Frise, V. Kaynig, M. Longair, T. Pietzsch, S. Preibisch, et al. 2012. Fiji: an open-source platform for biological-image analysis. *Nature Methods* 9: 676–682.

Schneider, C. A., W. S. Rasband, and K. W. Eliceiri. 2012. NIH Image to ImageJ: 25 years of image analysis. *Nature Methods* 9: 671–675.

Simeone, C., M. P. Maneta, Z. A. Holden, G. Sapes, A. Sala, and S. Z. Dobrowski. 2018. Coupled ecohydrology and plant hydraulics modeling predicts ponderosa pine seedling mortality and lower treeline in the US northern Rocky Mountains. *New Phytologist* 221: 1814–1830.

Sperry, J. S., J. R. Donnelly, and M. T. Tyree. 1988. A method for measuring hydraulic conductivity and embolism in xylem. *Plant, Cell & Environment* 11: 35–40.

Tyree, M. T., and M. H. Zimmermann. 2002. Xylem structure and the ascent of sap, 2nd ed. Springer, New York, NY, USA.

Urli, M., A. J. Porte, H. Cochard, Y. Guengant, R. Burlett, and S. Delzon. 2013. Xylem embolism threshold for catastrophic hydraulic failure in angiosperm trees. *Tree Physiology* 33: 672–683.

Wang, J., J. Feng, B. Chen, P. Shi, J. Zhang, J. Fang, Z. Wang, et al. 2016. Controls of seed quantity and quality on seedling recruitment of smith fir along altitudinal gradient in southeastern Tibetan Plateau. *Journal of Mountain Science* 13: 811–821.

Zavitkovski, J., and W. K. Ferrell. 1968. Effect of drought upon rates of photosynthesis, respiration, and transpiration of seedlings of two ecotypes of Douglas-fir. *Botanical Gazette* 129: 346–350.